Hyperfine interaction and magnetoresistance in organic semiconductors

Y. Sheng,[1] T. D. Nguyen,[1] G. Veeraraghavan,[2] Ö. Mermer,[1] M. Wohlgenannt,[1,*] S. Qiu,[3] and U. Scherf[3]
[1]*Department of Physics and Astronomy and Optical Science and Technology Center, University of Iowa, Iowa City, Iowa 52242-1479, USA*
[2]*Department of Electrical and Computer Engineering and Optical Science and Technology Center, University of Iowa, Iowa City, Iowa 52242-1595, USA*
[3]*Fachbereich Chemie, Makromolekulare Chemie, Bergische Universität Wuppertal, D-42097 Wuppertal, Germany*
(Received 22 February 2006; revised manuscript received 9 May 2006; published 26 July 2006)

We explore the possibility that hyperfine interaction causes the recently discovered organic magnetoresistance (OMAR) effect. We deduce a simple fitting formula from the hyperfine Hamiltonian that relates the saturation field of the OMAR traces to the hyperfine coupling constant. We compare the fitting results to literature values for this parameter. Furthermore, we apply an excitonic pair mechanism model based on hyperfine interaction, previously suggested by others to explain various magnetic-field effects in organics, to the OMAR data. Whereas this model can explain a few key aspects of the experimental data, we uncover several fundamental contradictions as well. By varying the injection efficiency for minority carriers in the devices, we show experimentally that OMAR is only weakly dependent on the ratio between excitons formed and carriers injected, likely excluding any excitonic effect as the origin of OMAR.

DOI: 10.1103/PhysRevB.74.045213 PACS number(s): 73.50.−h, 73.43.Qt

I. INTRODUCTION

Research of organic π-conjugated materials has largely been motivated by device applications such as organic light-emitting diodes (OLEDs),[1] field-effect transistors,[2] and photovoltaic cells,[3] i.e., it has been dominated by studies of charge transport and photophysics. Recently, there has been growing interest in spin[4–7] and magnetic-field effects (MFE)[8–19] in these materials. We recently discovered[8] a large, low field (up to 10% at 10 mT and 300 K) magnetoresistive effect in OLEDs, which we dubbed organic magnetoresistance (OMAR). In addition to its potential applications, OMAR poses a significant scientific puzzle since it is, to the best of our knowledge, the only known example of large room-temperature magnetoresistance in nonmagnetic materials with the exception of narrow-gap high-mobility materials.[20] Independently, Frankevich and co-workers[21,22] and Kalinowski and co-workers[12,23] studied the effect of magnetic fields on excitonic processes that occur in OLEDs, such as photoconductivity, electroluminescence (EL), and exciton dissociation at the electrodes. They explained their findings using a model where the applied magnetic field reduces the effect of the hyperfine interaction between electron/hole spin and the hydrogen nuclei in the organic molecules. We will refer to this work as the excitonic pair mechanism model, which will be treated in detail in Sec. IV C. Magnetic field effects in measurements of delayed fluorescence in organic solutions[24,25] have been interpreted using a similar model. Since the characteristic magnetic field scale in these experiments is similar to that of OMAR, the question naturally arises whether OMAR could also be caused by hyperfine interaction.

In the present work, we examine, among other things, whether the pair mechanism model as a particular embodiment of hyperfine interaction can explain OMAR. For this purpose, we recast this model into a form suitable for discussing the whole body of experimental MFE data, including both EL and transport measurements. We find that whereas this model can explain a few key aspects of the experimental data, it leads to several serious contradictions with experiment, especially in relation to the magnetotransport data. We trace the origin of these contradictions to the fact that this model treats the spin-dynamics of neutral polaron pairs that do not significantly affect the current. Furthermore, we show experimentally that the magnitude of OMAR depends only weakly on the ratio, η_1, between excitons formed and charge carriers injected into the devices. In our opinion, this shows that any model based on excitonic processes fails to explain OMAR. However, our study leads to insights into the hyperfine interaction in organics that are valid beyond the pair mechanism model.

II. EXPERIMENTAL

We first describe the sources for the various organic semiconductors we used in our study. The π-conjugated polymer polyfluorene (PFO) was purchased from American Dye Source, Inc. The methyl-substituted ladder-type poly(*p*-phenylene) (MeLPPP) polymer was synthesized as described elsewhere.[26] The π-conjugated small molecule tris-(8-hydroxyquinoline) aluminum(Alq_3) was purchased from H. W. Sands Corporation.

The fabrication of the organic sandwich devices started with glass substrates coated with 40 nm of indium-tin-oxide (ITO), purchased from Delta Technologies. The conducting polymer Poly (3,4-ethylenedioxythiophene)-poly (styrenesulfonate) (PEDOT), purchased from H. C. Starck, was spin-coated at 2000 rpm on top of the ITO to provide an efficient hole injecting electrode. All other manufacturing steps were carried out in a nitrogen glove box. The active polymer film was spin-coated onto the substrate from a chloroform solution. The small molecular film layers were made by thermal evaporation at a rate of $\approx$0.05 nm/s. The cathode, either Ca (with an Al capping layer), Al, or Au, was then deposited by

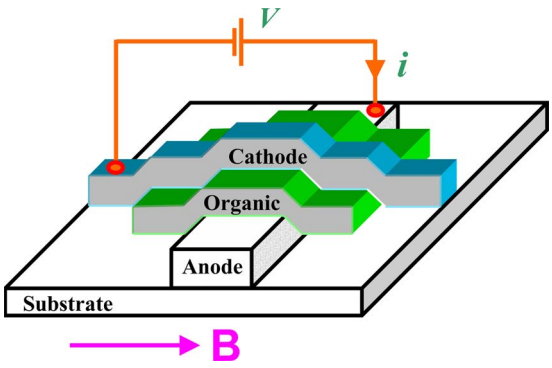

FIG. 1. (Color online) A schematic drawing of the device and the magnetoresistance experiment.

thermal (Ca) or electron beam evaporation (Al, Au) at a base pressure of $\approx 1 \times 10^{-6}$ mbar on top of the organic thin films. The device area was ≈ 1 mm^2 for all devices. The general device structure used for our measurements was metal/organic semiconductor/metal (see Fig. 1).

A schematic drawing of the device and the experiment is shown in Fig. 1. The samples were mounted on the cold finger of a closed-cycle helium cryostat located between the poles of an electromagnet to allow the devices to be operated in dynamic vacuum. The magnetoconductance ratio, $\Delta I/I$, was determined by measuring the current, I, at a constant applied voltage, V, for different magnetic fields, B. The EL of the devices was measured with a photomultiplier tube that was located ≈ 10 cm outside the magnet poles and was shielded from the magnetic field using high-saturation mu-shield foil. All the reported data are for room temperature.

III. EXPERIMENTAL RESULTS: MAGNETIC FIELD EFFECT ON CURRENT AND ELECTROLUMINESCENCE

First we present the main experimental observations relating to OMAR in two example materials: one is a π-conjugated polymer, the other a small molecule. OMAR devices have the unique property of showing large magnetoresistance while being also highly electroluminescent. Figures 2 and 3 show $\Delta I/I$ and $\Delta EL/EL$ versus B in a PEDOT/PFO/Ca and PEDOT/Alq_3/Ca device, respectively, measured at a constant voltage. These data show that the MFE exists both in the electric and luminescent measurements with comparable magnitude. Note that the shapes of $(\Delta I/I)(B)$ and $(\Delta EL/EL)(B)$ are equivalent and that both scale in the same manner upon changing V. Both effects, therefore, share a common origin. EL and I are related through

$$EL \propto \eta I, \tag{1}$$

where η is the EL quantum efficiency. The EL process is commonly broken down into three steps,[27] and η can accordingly be written as

$$\eta = \eta_1 \eta_2 \eta_3, \tag{2}$$

where η_1 is the fraction of the injected carriers that form electron-hole pairs, η_2 is the fraction of the total number of excitons that are singlets, and η_3 is the singlet emission quantum efficiency. We will use these insights later when we apply the pair mechanism model to OMAR. Before proceeding, however, we want to analyze the experimental evidence that supports the claim that the hyperfine interaction causes the magnetic field effect on electroluminescence (MEL) and OMAR.

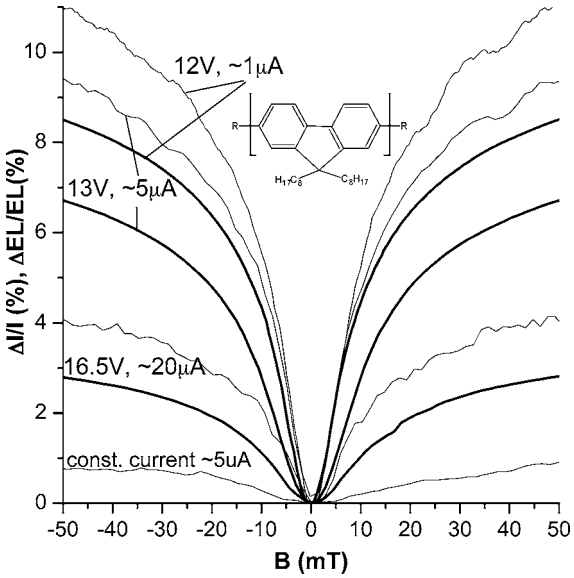

FIG. 2. Magnetic-field effect on current, I (bold) and EL in a PEDOT/PFO(≈100 nm)/Ca device measured at several different constant voltages at room temperature.

IV. DISCUSSION

Figure 4 shows a summary of measured OMAR traces, taken from our previous publication,[10] in PEDOT/organic layer/Ca devices employing several different organic layers.

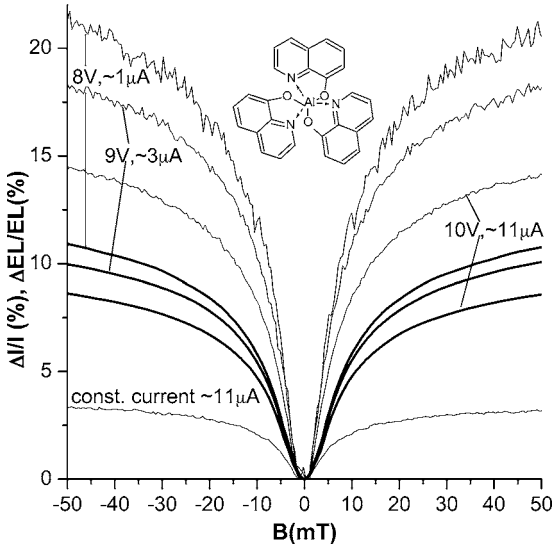

FIG. 3. Magnetic-field effect on current, I (bold) and EL in a PEDOT/Alq_3 (≈100 nm)/Ca device measured at several different constant voltages at room temperature.

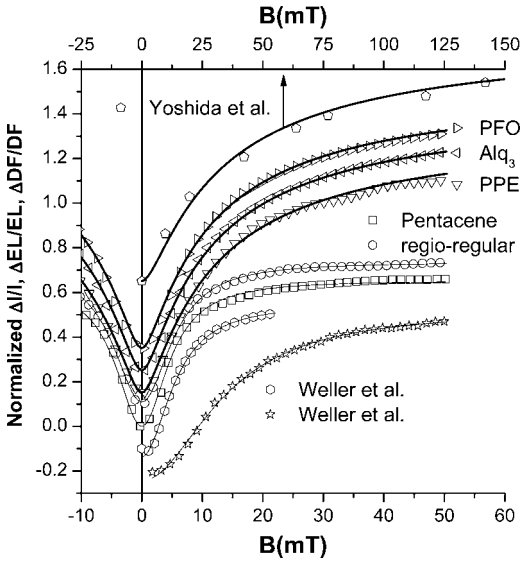

FIG. 4. Normalized OMAR traces, $\Delta I/I$, in PEDOT/organic layer/Ca devices, with PFO, Alq_3, poly(phenylene-ethynelene) (PPE), pentacene and regio-regular P3HT as the organic layers, taken from Ref. 10. For comparison, poly(3-hexylthiophene) (P3HT) data on the normalized MEL effect, $\Delta EL/EL$, in a poly(phenylene-vinylene) OLED measured by Yoshida *et al.* (Ref. 15) and that on the triplet photoyield in solutions (measured as a change, $\Delta DF/DF$, in delayed fluorescence) of organic materials measured by Weller *et al.* (Refs. 24 and 25) are also shown. The data are shown as scatter plots as detailed in the legend. The solid curves are fits using empirical laws of the forms $[B/(|B|+B_0)]^2$ (thicker lines) and $B^2/(B^2+B_0^2)$ (thinner lines). Please note that the data by Yoshida *et al.* and the corresponding fit refer to the upper x axis, whereas all other data refer to the lower x axis. The data sets were offset along the y axis for clarity.

The traces of the various data sets have been normalized (with respect to the y axis) to achieve a suitable graphical representation. The solid curves are fits using empirical laws of the forms $[B/(|B|+B_0)]^2$ (thicker lines) and $B^2/(B^2+B_0^2)$ (thinner lines); the values for the fitting parameter, B_0, are given in Table I. These empirical laws were introduced by us in a previous publication[10] and yield excellent one-parameter fits. For comparison, data on the MEL effect in a poly(phenylene-vinylenene) OLED measured by Yoshida *et al.*[15] and those on the triplet photoyield in organic solutions measured by Weller *et al.*[24,25] are also shown. Figure 4 shows that the data by Yoshida *et al.* and Weller *et al.* can also be fitted accurately by our empirical laws, suggesting a common origin of OMAR and other MFE data. Since Yoshida *et al.* and Weller *et al.* have interpreted their data in terms of the pair mechanism (hyperfine interaction) model, this suggests that OMAR is also caused by hyperfine interaction. As a matter of fact, Weller and co-workers[24,25] have directly shown through transient measurements of the delayed fluorescence in solutions of organic materials that a weak magnetic field can modulate the spin multiplicity within 10–20 ns after optical excitation, consistent with the hyperfine coupling strength. Furthermore, Schulten *et al.*[28] showed that the width of the MFE traces can be calculated from first principles based on the hyperfine coupling constants. However, Schulten's work did not specify an analytical result for the dependence of the MFE on B, and the origin of the simple, analytical fitting formulas, $[B/(|B|+B_0)]^2$ and $B^2/(B^2+B_0^2)$, is not yet well established. We have therefore performed a simplified calculation of the dependence of the MFE on B (see the Appendix) where we show that the origin of the empirical law, $B^2/(B^2+B_0^2)$, can be readily understood from the hyperfine Hamiltonian. We note that this formula is closely related to the Lorentzian function $B_0^2/(B^2+B_0^2)$. However, we have not yet been able to deduce the other empirical law, $B^2/(|B|+B_0)^2$, from the hyperfine Hamiltonian.

TABLE I. Function and parameter values used for fits in Fig. 4.

Fitting function: $B^2/(B^2+B_0^2)$	
material name	B_0 (mT)
regio-regular P3HT	5.1
pentacene	5.8
Weller *et al.* 1	5.7
Weller *et al.* 2	13.7
Fitting function: $(B/(\|B\|+B_0))^2$	
material name	B_0 (mT)
PFO	5.4
Alq_3	5.4
PPE	5.5
Yoshida *et al.*	14

A. Comparison between theoretical predictions based on hyperfine coupling and experimental results for the width of OMAR traces

The calculation presented in the Appendix, combined with a formula given by Schulten,[29] gives $B_0=\sqrt{3}(\Sigma_i a_{H,i}^2)^{1/2}$ for nuclear spin 1/2. This makes it possible to compare the measured values for B_0 with values calculated from the published values for the hyperfine splitting constants, $a_{H,i}$, in the electron-spin resonance spectra of the organic molecules (see, e.g., Refs. 30 and 31), where the index i labels the individual hydrogen nuclei. As a matter of fact, the width of the Weller *et al.*[24] data numerically coincides with Schulten's formula with pretty good accuracy. However, for our OMAR data the experimental width is considerably greater than the calculated one. For pentacene, for example, we calculate $B_0=1.8$ mT from the published values of the isotropic hyperfine coupling constants,[31] whereas the experimental value is $B_0=5.8$ mT (see Table I). Indeed, the fact that the widths of the MFE traces in OLEDs are much wider than expected from hyperfine coupling has already been recognized by Yoshida *et al.*,[15] who therefore suggested that this is a result of lifetime broadening. Our experiments, however, exclude this possibility: The pair lifetime should be a sensitive function of temperature and should vary considerably between different materials in contradiction with experiment (see Ref. 10 and Fig. 4). Although we have been unable to find a

convincing explanation for this discrepancy, it is possible that hyperfine coupling with hydrogen nuclei of neighboring molecules in the densely packed films and anisotropic hyperfine coupling may account for the excess width.

A further serious disagreement between theoretical expectation based on hyperfine coupling and experimental results is evident from the observation that B_0 is similar in both small molecules and polymers. This is unexpected because McConnell's relationship[32] states that $a_{H,i}=Q\rho_i$, where ρ_i is the spin density (in units of spins/site) at site, i, and $Q \approx 3$ mT for conjugated molecules.[31] For a polymer with N repeat units, we therefore have

$$a_H^2 = \sum (Q\rho_i)^2 \approx N\sum{}' (Q\rho_i)^2 \approx N\sum{}' (Q\rho_i'/N)^2, \quad (3)$$

$$a_H \propto N^{-1/2}, \quad (4)$$

where Σ denotes a sum over all nuclei in the polymer, whereas Σ' is a sum only over a single repeat unit. ρ_i is the spin density at nucleus, i, whereas ρ_i' is the spin density at nucleus, i, in the corresponding monomer. This result implies that the MFE cones should be considerably narrower in polymers than in small molecules such as Alq_3, in contradiction with the experimental results (see Fig. 4).

B. Potential implication of hyperfine coupling to organic spintronics applications

The discovery of OMAR and its possible relation to hyperfine interaction illustrates the importance of the study of spin-dynamics and hyperfine interaction in relation to transport phenomena. In particular, we believe that the existence of hyperfine interaction has fundamental implications for the currently emerging field of organic spintronics.[5,6] Since hyperfine coupling leads to time evolution of the electron spin (see the Appendix) and since the local nuclear spin configuration is different for each molecule in the film, hyperfine coupling will lead to spin decoherence. The relevant decoherence time scale, T_2^*, for a spin ensemble is given by

$$T_2^* \approx \frac{\hbar}{g\mu_B a_H} \approx 10 \text{ ns}, \quad (5)$$

where the symbols in the equation have their usual meanings (see the Appendix). The value for a_H is known for many molecules from electron-spin resonance spectroscopy,[30,31] and assuming that OMAR is indeed caused by hyperfine interaction, we would have $a_H \approx B_0$. Upon applying $B > a_H$, however, this decoherence mechanism is suppressed because the electronic Zeeman term in the hyperfine Hamiltonian effectively pins the spin orientation (see the Appendix). This small value for T_2^* appears at first sight to contradict much larger T_2 values for π-conjugated materials determined by electron spin-resonance measurements.[33] However, these measurements are always performed under large applied fields and are therefore not sensitive to the decoherence mechanism we propose here. Assuming the drift term to be dominant in OLEDs, we therefore obtain for the spin-transport length, λ,

$$\lambda \approx \mu F T_2^* \approx 1 \text{ nm}, \quad (6)$$

where we have used $\mu = 10^{-4}$ cm^2(V s)$^{-1}$ and $F = 10^5$ V cm^{-1} for typical mobility and electric field values, respectively. This result clearly shows that hyperfine interaction may seriously limit the spin-transport properties of organic semiconductors. This surprisingly small spin-transport length appears to be at variance with a recent report of giant magnetoresistance in spin valves with organic semiconductor spacers of more than 100 nm thickness.[6] However, close inspection of these data shows that no spin-valve effect is present at zero applied field (their data are reported with 2.5 mT resolution, and a spin-valve effect exists at 2.5 mT, a field that may be large enough to pin the spins). Our analysis of decoherence leads us to believe that no organic spin-valve effect should be observable at spacer internal fields smaller than a_H, unless other, currently unknown pinning mechanisms are active, or high-mobility organic spacers are used.

C. Excitonic pair mechanism model

Next, we examine whether OMAR can be explained by the excitonic pair mechanism model that was applied to MEL in OLEDs by Frankevich[21] and Kalinowski.[12] Since, as we have shown in Sec. III, MEL and OMAR likely share a common origin, it is natural to ask whether this model can explain OMAR. When electrons and holes are injected from the cathode and anode into the organic layer, they form negative and positive polarons, respectively.[34] As long as the distance between positive and negative carriers is larger than the Coulomb capture radius, they do not feel each other's attraction, and we refer to them as free charges. We assume that at separations less than the capture radius, the carriers are organized in bound polaron pairs (PP). As the separation becomes less than the single-particle wave function extend, the exchange interaction becomes important and the pair has to be represented by a single, properly symmetrized, wave function. We refer to this as an exciton. We note that the pair mechanism model is an example of a spin-dependent effect that does not require (thermal) spin-polarization, which would be consistent with the relative temperature insensitivity of OMAR.[8–10] One way of understanding this is to realize that, since the carriers form pairs, the ensemble consists of two spins only and very large effective spin-polarization is automatically achieved. The formation of pairs is therefore essential to this model.

Closely following the treatment by Frankevich,[21] we now formulate the appropriate rate equations. The relevant levels and transition rates are shown in Fig. 5. ^1PP, $^3PP_0$, $^3PP_+$, $^3PP_-$ denote the pair populations, where the superscript (subscript) denotes multiplicity (spin projection). The basic idea of the pair mechanism model is that the multiplicity of the PPs changes with time due to spin dynamics induced by the hyperfine interaction[28,29,35,36] (see the Appendix). We denote the rate of conversion between the isoenergetic ^1PP and $^3PP_0$ as k_{HF_0}, and that between other PP as k_{HF}. If $B=0$, then $k_{HF}=k_{HF_0}$. An applied B field leads to Zeeman splitting, ΔE, between levels of different spin projection. If $\Delta E > \hbar k_{HF_0}$, then $k_{HF}=0$, however k_{HF_0} remains unchanged. The simplest

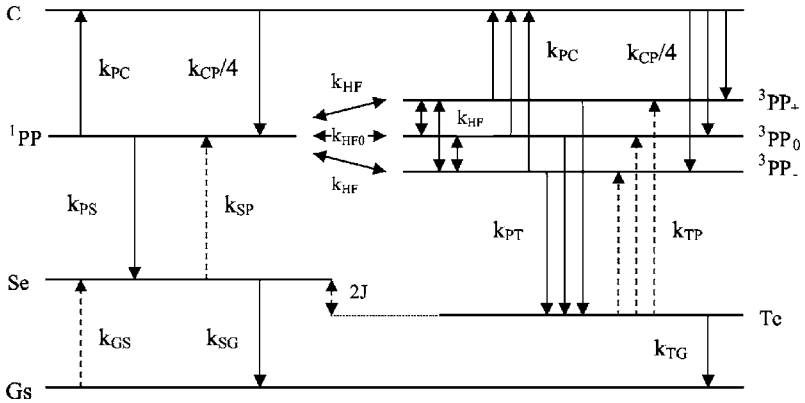

FIG. 5. The schematic energy level diagram illustrates the simplest possible pair mechanism model, which includes three different species: (i) free charges with population C, (ii) polaron pairs PPs, and (iii) singlet Se and triplet excitons Te with large exchange interaction, J. Gs denotes the ground state. The various transition rates are indicated. The dashed arrows denote transitions that we neglect in our model.

possible model for explaining the magnetic field effect of I and EL requires rate equations for three different species, namely (i) free charges that carry the current, (ii) pairs, such that it becomes meaningful to talk about singlet and triplet states, and (iii) excitons that, by virtue of their large exchange energy, furnish the model with spin-dependent pair recombination rates.[4,37] We note that pairs and excitons do not contribute to the current, because of their overall neutrality. The various rate equations are given by (see Fig. 5)

$$G_C + k_{PC}\left(\sum {}^iPP\right) - k_{CP}C = 0, \tag{7}$$

$$\frac{1}{4}k_{CP}C + k_{\mathrm{HF}_0}({}^3PP_0 - {}^1PP) + k_{\mathrm{HF}}({}^3PP_+ - {}^1PP) + k_{\mathrm{HF}}({}^3PP_- - {}^1PP) - (k_{PC} + k_{PS}){}^1PP = 0. \tag{8}$$

The first rate equation is for the free charges, C. G_C is the generation rate for C, which is equal to the rate of carrier injection minus the rate of emission of carriers at the electrodes. The second equation is the rate equation for singlet PPs; three additional equations similar to Eq. (8) are necessary to describe the triplet PPs. We neglected the upwards transitions k_{SP}, k_{TP}, k_{GS} (dashed arrows in Fig. 5) to simplify the rate equations. We obtain the following solutions to the rate equations:

$$\frac{\Delta I}{I} = \eta_1 \frac{\frac{k_{PC}}{k_{PT}}(1-r)^2}{\left(4\frac{k_{PC}}{k_{PT}} + r + 3\right)\left[\frac{k_{PC}}{k_{PT}}(r+3) + 2(r+1)\right]}, \tag{9}$$

$$\frac{\Delta EL}{EL} = \frac{1-r}{\frac{k_{PC}}{k_{PT}}(r+3) + 2(r+1)}, \tag{10}$$

where we have used $EL \propto {}^1PP$ and $I \propto C$; $r \equiv k_{PS}/k_{PT}$.[4] We have used $k_{\mathrm{HF}_0} \gg k_{PS}, k_{PT}, k_{PC}$ (see Sec. IV A). We will now show that these results are in clear contradiction with experiments. Equation (9) shows that $\Delta I/I$ is always positive in this model, in contradiction with the experimental results where both positive and negative magnetoconductance is observed.[10] Furthermore, it is seen that $\Delta I/I$ is a second-order effect, whereas $\Delta EL/EL$ appears in first order in $(1-r)$. This contradicts the experimental observation that both effects are of similar magnitude and that the two effects scale in a manner that conserves the ratio between them upon changing the voltage (see Figs. 2 and 3). Most importantly, Eq. (9) shows that $\frac{\Delta I}{I} \propto k_{PC}/k_{PT}$ for $k_{PC} \ll k_{PT}$ and $\frac{\Delta I}{I} \propto k_{PT}/k_{PC}$ for $k_{PC} \gg k_{PT}$. Therefore, the magnetoconductance should always be very small except for the singular case that $k_{PC} \approx k_{PT}$. This conclusion arises because free charges, the only current-carrying species in the model, do not directly participate in the spin-dependent reactions or the hyperfine-induced intersystem crossing. In particular, when $k_{PC}/k_{PT} \gg 1$, most polarons exist as free charges and the pair concentration and therefore the MFE are small. When $k_{PC}/k_{PT} \ll 1$, the pair concentration and therefore the MFE are large, but this does not affect the current because the pairs do not dissociate.

V. EXPERIMENTAL RESULTS: DEPENDENCE OF THE MAGNETOCONDUCTANCE RATIO ON THE MINORITY CARRIER INJECTION EFFICIENCY

In this section, we determine experimentally whether OMAR is related to an excitonic effect or not. This is possible, since η_1 that appears in Eq. (9) can be varied experimentally by several orders of magnitude. One can control the injection of minority charge carriers by varying the corresponding electrode materials. The number of excitons formed in the device is proportional to the minority carrier concentration, whereas the current density is determined mostly by the majority carriers. This idea can be easily realized in hole-dominated PFO devices by choosing cathode (top electrode) materials with different work functions. Whereas most polymers are hole transporters, Alq_3 is an electron transporter,[38] meaning its majority carriers are electrons. It is difficult in practice to fabricate electron-only Alq_3 devices because efficient electron injection requires reactive metals such as Ca. We found, e.g., in a $Ca/Alq_3/Ca$ device, that the bottom Ca electrode oxidizes quickly before and after evaporating Alq_3 on top of it. So, instead of Alq_3 devices we studied a second polymer, MeLPPP (see Fig. 7, inset) in addition to PFO, to show that the conclusions we draw are not limited to a particular choice of polymer. MeLPPP is a suitable choice, because it shows, like PFO devices, large OMAR as well as intense EL.

We fabricated and measured PFO and MeLPPP devices using Ca, Al, and Au as cathode materials. We note that

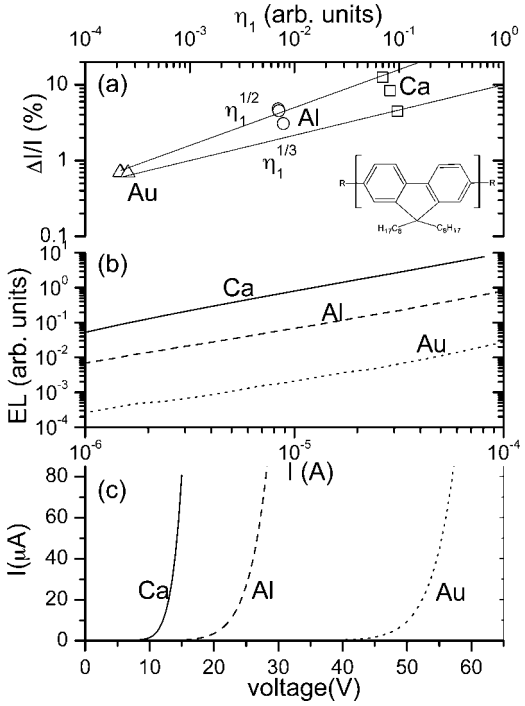

FIG. 6. (a) $\Delta I/I$ at $B=100$ mT in several PEDOT/PFO ($\approx$150 nm)/cathode devices with Ca, Al, or Au as the cathode as a function of the exciton/carrier ratio η_1. (b) EL as a function of current. (c) Current-voltage (I-V) characteristics. All data were obtained at room temperature.

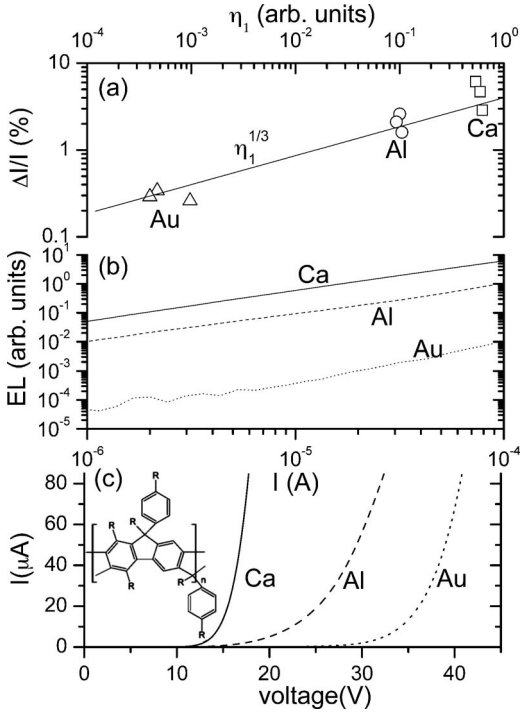

FIG. 7. (a) $\Delta I/I$ at $B=100$ mT in several PEDOT/MeLPPP ($\approx$150 nm)/cathode devices with Ca, Al, or Au as the cathode as a function of the exciton/carrier ratio η_1. (b) EL as a function of current. (c) Current-voltage (I-V) characteristics. All data were obtained at room temperature.

whereas only data points for a single device of each type are shown, the reported experiments were repeated several times and very reproducible results were obtained. Figures 6 and 7 show the current-voltage (I-V) characteristics [Figs. 6(c) and 7(c)], the measured EL intensity as a function of I [Figs. 6(b) and 7(b)], and the magnitude of $\Delta I/I$ as a function of η_1 [Figs. 6(a) and 7(a)]. The exciton/carrier ratio, η_1, was inferred from the data shown in panel (b), where we found that the magnitude of EL, at a given current, in Ca devices is about one order of magnitude larger than that in Al devices, and about three orders of magnitude larger than in Au devices. This is well known[27] to result from the mismatch of the cathode work function and the polymer's conduction band in the case of Al and Au cathodes. Correspondingly, η is one (three) order of magnitude lower in Al (Au) devices compared to Ca devices. Since η_2 and η_3 in Eq. (2) are (fixed) properties of the excitons[39] in each organic material, we simply use η as a measure of the exciton/carrier ratio, η_1, of the various devices.

Figures 6(a) and 7(a) show that the magnitude of $\Delta I/I$ increases as η_1 increases in both PFO and MeLPPP devices (results for three choices of the current, specifically approximately 1 μA, 10 μA and 100 μA, are shown for each device). At first sight this trend seems to confirm an excitonic origin of OMAR. However, closer inspection shows that the η_1 dependence is much weaker than expected. Whereas a linear dependence on η_1 is expected for an excitonic effect, we find $\Delta I/I \propto \eta_1^{\alpha}$, with α ranging from 1/3 to 1/2. If, however, OMAR is not related to an excitonic effect, we would have expected no dependence at all, which does not match the measurements either. However, the observed weak dependence is not unexpected: It is possible that the interface resistance of polymer/Au is larger than that of polymer/Ca, resulting in additional resistance that is not subject to OMAR. Previous studies (Ref. 40 and references therein) report that Au indeed forms a non-Ohmic top contact, possibly because the wetting of Au and therefore the physical contact is inferior, or because Au deposition, which has to be evaporated at a much higher temperature than Ca, leads to damage of the underlying polymer surface. Moreover, in unipolar devices, space-charge-limited current conditions occur that are possibly unfavorable for OMAR. In bipolar devices, however, the space charge of the two carrier types partially cancel each other. The fact that changing the cathode material leads to additional effects, rather than merely changing η_1, is shown in Figs. 6(c) and 7(c): It is seen that Al and Au cathode devices show a significantly increased device resistance, probably due to the above-mentioned parasitic resistance contributions. We have, however, been unable to come up with any probable or improbable explanation for how the dependence on η_1 could be sublinear in an excitonic model. We could imagine superlinear behavior, if the spin-dependent reactions are bimolecular. Our measurements therefore show that OMAR is most likely not related to an excitonic effect.

VI. CONCLUSION

We have explored the possibility that hyperfine interaction causes the recently discovered organic magnetoresistance effect using both experimental data and theoretical models. We

show that both OMAR and other kinds of magnetic field effect data in organics can be fitted using the empirical laws $B^2/(B^2+B_0^2)$ or $B^2/(|B|+B_0)^2$, dependent on material. The only fitting parameter, B_0, assumes values that, at least at first sight, seem typical of hyperfine interaction. This suggests that OMAR is caused by hyperfine interaction. We succeeded in deriving the empirical law $B^2/(B^2+B_0^2)$ from the standard hyperfine Hamiltonian. We obtain similar experimental values for B_0 both in polymers and small molecules and show that this is inconsistent with hyperfine coupling. We also showed that hyperfine interaction may seriously limit the spin-transport length, which is of primary importance in spintronics applications.

In order to further test the hyperfine interaction hypothesis, we examined a pair mechanism model, suggested previously by other authors to explain various excitonic magnetic field effects in organics. Whereas this model correctly accounts for several key experimental observations, such as the Lorentzian lineshape of OMAR, we found several fundamental contradictions with the existing experimental data as well: This model yields only a small and necessarily positive magnetoconductance effect, whereas experimentally a large effect is found, either of positive or negative sign. It is found that whereas $\Delta EL/EL$ is a first-order effect, $\Delta I/I$ appears only in second order, in contradiction to the experimental observation that they are of similar magnitude. We trace the origin of the failure of the model in explaining OMAR to the fact that it considers the spin-dynamics of neutral polaron pairs, which, in first order, do not contribute to the current.

By varying the injection efficiency for minority carriers in the devices, we show experimentally that $\Delta I/I$ is only weakly dependent on the EL quantum efficiency: $\Delta I/I \propto \eta_1^{\alpha}$, with α ranging from 1/3 to 1/2. This dependence is unexpectedly weak if the effect is of an excitonic origin. This observation confirms the conclusion from the modelling that OMAR is not due to an excitonic effect.

ACKNOWLEDGMENTS

We acknowledge fruitful and inspiring discussions with M. E. Flatté, C. E. Pryor, and K. Schulten. This work was supported by NSF Grant No. ECS 04-23911.

APPENDIX: LORENTZIAN SHAPE OF MAGNETIC-FIELD EFFECT TRACES DEDUCED FROM THE HYPERFINE HAMILTONIAN

Here we will show that the empirical fitting formula $\Delta I/I \propto B^2/(B^2+B_0^2)$ can be substantiated through a simple calculation to be presented in the following. A similar calculation can be found in Ref. 41. Here we expand on this calculation and cast it in a form that applies directly to the present work. The model considers the standard hyperfine Hamiltonian,

$$\hat{H} = \omega_0 \hat{S}_z + \frac{a}{\hbar} \hat{\vec{S}} \hat{\vec{I}}, \tag{A1}$$

containing the electronic Zeeman energy and the hyperfine interaction between a single electronic and nuclear dipole. $\omega_0 = \frac{g\mu_B B}{\hbar}$, where $g \approx 2$ is the electronic g-factor and μ_B is the electronic Bohr magneton, $\vec{S}$ and $\vec{I}$ are the electronic and nuclear spin (assumed to be 1/2), respectively, and a is a measure (in units of frequency) of the hyperfine interaction strength. The z axis is chosen to coincide with the direction of B. The Hamiltonian will be written in matrix form where we use the following basis vectors: $|\Uparrow\uparrow\rangle$, $|\Downarrow\uparrow\rangle$, $|\Uparrow\downarrow\rangle$, and $|\Downarrow\downarrow\rangle$. The boldface arrow denotes the z component of the electronic spin, whereas the second arrow denotes that of the nuclear spin. We obtain the following result:

$$\hat{H} = \hbar \begin{bmatrix} \frac{\omega_0}{2} + \frac{a}{4} & 0 & 0 & 0 \\ 0 & -\frac{\omega_0}{2} - \frac{a}{4} & \frac{a}{2} & 0 \\ 0 & \frac{a}{2} & \frac{\omega_0}{2} - \frac{a}{4} & 0 \\ 0 & 0 & 0 & -\frac{\omega_0}{2} + \frac{a}{4} \end{bmatrix}. \tag{A2}$$

It is evident from the form of $\hat{H}$ that $|\Uparrow\uparrow\rangle$ and $|\Downarrow\downarrow\rangle$ are eigenstates and therefore do not evolve with time other than through the trivial phase factor. However, $|\Downarrow\uparrow\rangle$ and $|\Uparrow\downarrow\rangle$ are mixed with each other through the off-diagonal matrix element. For simplicity, we will now consider the time evolution of the $|\Uparrow\downarrow\rangle$ state only. It turns out that a calculation of the time evolution of the most general state vector and subsequent averaging over all electronic and nuclear spin orientations leads to similar results. To obtain the time evolution operator, we perform a matrix exponentiation,

$$\hat{U} = \exp\left(\frac{\hat{H}t}{i\hbar}\right). \tag{A3}$$

Next we calculate the expectation value of $\hat{S}_z$ as a function of time,

$$S_z(t) = \langle \Uparrow\downarrow \hat{U} | \hat{S}_z | \hat{U} \Uparrow\downarrow \rangle. \tag{A4}$$

We obtain the following result (in units of $\hbar/2$):

$$S_z(t) = \frac{\omega_0^2}{\omega_0^2 + a^2} + \frac{a^2}{\omega_0^2 + a^2} \cos\sqrt{\omega_0^2 + a^2}\, t. \tag{A5}$$

Next we consider the case of a pair of spins, each of which is subject to a separate Hamiltonian of form Eq. (A1). For simplicity, we will treat the time evolution of the initial state $|\Uparrow\uparrow\rangle_1 |\Uparrow\downarrow\rangle_2$ only. Since the first spin is in an eigenstate, it will not evolve with time, whereas the second spin's time evolution will be governed by Eq. (A3). We obtain, therefore, for the total spin (in units of $\hbar$),

$$S_z^{1+2}(t) = \frac{1}{2}\left(1 + \frac{\omega_0^2}{\omega_0^2 + a^2} + \frac{a^2}{\omega_0^2 + a^2} \cos\sqrt{\omega_0^2 + a^2}\, t\right) \tag{A6}$$

$$= \frac{1}{2} + \frac{1}{2}(p_P - p_{AP}), \tag{A7}$$

where p_P and p_{AP} are the probability for finding the pair in a parallel or antiparallel state, respectively. It is seen that $S_z^{1+2}(t)$ oscillates with time and that the peak-to-peak modulation depth is given by $\frac{a^2}{\omega_0^2+a^2}$. At large B, $S_z^{1+2}(t)$ remains close to 1 at all times although it performs a high-frequency (but small-amplitude) oscillation. At small B, the frequency of the oscillation becomes smaller but its amplitude increases. The question arises whether the frequency or the amplitude of the oscillation is the correct measure for the spin-flip efficiency. Because experiment shows (see Sec. IV A) that the oscillation frequency is much larger than the pair recombination rate, γ, it is the time average of $S_z^{1+2}(t)$ that enters into the transition rate. Specifically, we may write

$$\gamma = \overline{p_P}\gamma_P + \overline{p_{AP}}\gamma_{AP} \tag{A8}$$

$$= \left(\frac{1}{2} + \frac{\omega_0^2}{2(\omega_0^2 + a^2)}\right)\gamma_P + \frac{a^2}{2(\omega_0^2 + a^2)}\gamma_{AP}, \tag{A9}$$

$$\frac{\Delta\gamma}{\gamma} \equiv \frac{\gamma(B) - \gamma(B=0)}{\gamma(B=0)} = \frac{\omega_0^2}{\omega_0^2 + a^2}\frac{\gamma_P - \gamma_{AP}}{\gamma_P + \gamma_{AP}}. \tag{A10}$$

γ_P and γ_{AP} are the recombination rates for parallel and antiparallel pairs, respectively. For a state initially in an antiparallel state, γ_P and γ_{AP} have to be exchanged in Eq. (A10).

Finally, we relate our results to the experimentally reported values, $a_H = \frac{\hbar a}{g\mu_B}$, for the hyperfine coupling strength,

$$\frac{\Delta\gamma}{\gamma} \propto \frac{B^2}{B^2 + a_H^2}. \tag{A11}$$

Schulten and co-workers[29] have shown that if the electron spin interacts with a large number of nuclear spins (as in the case of organic semiconductors), then the individual $a_{H,i}$ have to be added in a random-walk-like manner,

$$B_0 \to \sqrt{3}\left(\sum_i a_{H,i}^2\right)^{1/2}. \tag{A12}$$

*Electronic address: markus-wohlgenannt@uiowa.edu

[1] S. R. Forrest, Nature (London) **428**, 911 (2004).
[2] C. D. Dimitrakopoulos and P. R. L. Malenfant, Adv. Mater. (Weinheim, Ger.) **14**, 99 (2002).
[3] C. J. Brabec, N. S. Sariciftci, and J. C. Hummelen, Adv. Funct. Mater. **11**, 15 (2001).
[4] M. Wohlgenannt, K. Tandon, S. Mazumdar, S. Ramasesha, and Z. V. Vardeny, Nature (London) **409**, 494 (2001).
[5] V. Dediu, M. Murgia, F. C. Matacotta, C. Taliani, and S. Barbanera, Solid State Commun. **122**, 181 (2002).
[6] Z. H. Xiong, D. Wu, Z. V. Vardeny, and J. Shi, Nature (London) **427**, 821 (2004).
[7] B. Hu, Y. Wu, Z. Zhang, S. Dai, and J. Shen, Appl. Phys. Lett. **88**, 022114 (2006).
[8] T. L. Francis, Ö. Mermer, G. Veeraraghavan, and M. Wohlgenannt, New J. Phys. **6**, 185 (2004).
[9] Ö. Mermer, G. Veeraraghavan, T. Francis, and M. Wohlgenannt, Solid State Commun. **134**, 631 (2005).
[10] Ö. Mermer, G. Veeraraghavan, T. L. Francis, Y. Sheng, D. T. Nguyen, M. Wohlgenannt, A. Kohler, M. K. Al-Suti, and M. S. Khan, Phys. Rev. B **72**, 205202 (2005).
[11] Ö. Mermer, G. Veeraraghavan, T. L. Francis, and M. Wohlgenannt, "Weak localization and antilocalization in polymer sandwich devices", cond-mat/0312204 (unpublished).
[12] J. Kalinowski, M. Cocchi, D. Virgili, P. D. Marco, and V. Fattori, Chem. Phys. Lett. **380**, 710 (2003).
[13] J. Kalinowski, M. Cocchi, D. Virgili, V. Fattori, and P. Di Marco, Phys. Rev. B **70**, 205303 (2004).
[14] A. H. Davis and K. Bussmann, J. Vac. Sci. Technol. A **22**, 1885 (2004).
[15] Y. Yoshida, A. Fujii, M. Ozaki, K. Yoshino, and E. L. Frankevich, Fusion Sci. Technol. **426**, 19 (2005).
[16] G. Salis, S. F. Alvarado, M. Tschudy, T. Brunschwiler, and R. Allenspach, Phys. Rev. B **70**, 085203 (2004).
[17] C. Garditz, A. G. Muckl, and M. Colle, J. Appl. Phys. **98**, 104507 (2005).
[18] V. N. Prigodin, N. P. Raju, K. I. Pokhodnya, J. S. Miller, and A. J. Epstein, Adv. Mater. (Weinheim, Ger.) **14**, 1230 (2002).
[19] N. P. Raju, T. Savrin, V. N. Prigodin, K. I. Pokhodnya, J. S. Miller, and A. J. Epstein, J. Appl. Phys. **93**, 6799 (2003).
[20] R. Xu, A. Husmann, T. F. Rosenbaum, M.-L. Saboungi, J. E. Enderby, and P. B. Littlewood, Nature (London) **390**, 57 (1997).
[21] E. L. Frankevich, A. A. Lymarev, I. Sokolik, F. E. Karasz, S. Blumstengel, R. H. Baughman, and H. H. Horhold, Phys. Rev. B **46**, 9320 (1992).
[22] E. Frankevich, A. Zakhidov, K. Yoshino, Y. Maruyama, and K. Yakushi, Phys. Rev. B **53**, 4498 (1996).
[23] J. Kalinowski, J. Szmytkowski, and W. Stampor, Chem. Phys. Lett. **378**, 380 (2003).
[24] A. Weller, F. Nolting, and H. Staerk, Chem. Phys. Lett. **96**, 24 (1983).
[25] H. Staerk, W. Kühnle, and A. Weller, Chem. Phys. Lett. **118**, 19 (1985).
[26] U. Scherf and K. Müllen, Makromol. Chem. **112**, 489 (1991).
[27] R. H. Friend *et al.*, Nature (London) **397**, 121 (1999).
[28] K. Schulten, J. Chem. Phys. **82**, 1312 (1984).
[29] K. Schulten and P. Wolynes, J. Chem. Phys. **68**, 3292 (1978).
[30] F. Gerson and W. Huber, *Electron Spin Resonance Spectroscopy for Organic Radicals* (Wiley-VCH, Weinheim, 2003).
[31] I. C. Lewis and L. S. Singer, J. Chem. Phys. **43**, 2712 (1965).
[32] H. M. McConnel, J. Chem. Phys. **24**, 764 (1956).
[33] V. I. Krinichnyi, Synth. Met. **108**, 173 (2000).
[34] Z. V. Vardeny and X. Wei, *Handbook of Conducting Polymers II* (Marcel Dekker, New York, 1997), Chap. 22.
[35] E. Knapp and K. Schulten, J. Chem. Phys. **71**, 1878 (1979).
[36] U. E. Steiner and T. Ulrich, Chem. Rev. (Washington, D.C.) **89**,

51 (1989).
[37] M. Wohlgenannt and Ö. Mermer, Phys. Rev. B **71**, 165111 (2005).
[38] R. G. Kepler, P. M. Beeson, S. J. Jacobs, R. A. Anderson, M. B. Sinclair, V. S. Valencia, and P. A. Cahill, Appl. Phys. Lett. **66**, 3618 (1995).
[39] M. A. Baldo, D. F. O'Brien, M. E. Thompson, and S. R. Forrest, Phys. Rev. B **60**, 14422 (1999).
[40] A. J. Campbell and D. Bradley, J. Appl. Phys. **89**, 3343 (2001).
[41] K. M. Salikhov, *Spin Polarization and Magnetic Effects in Radical Reactions* (Elsevier, Budapest, 1984).